

# Discovery of Novel Acetohydroxyacid Synthase Inhibitors as Active Agents against *Mycobacterium tuberculosis* by Virtual Screening and Bioassay

Di Wang,<sup>†,||</sup> Xuelian Zhu,<sup>‡,||</sup> Changjun Cui,<sup>§,||</sup> Mei Dong,<sup>†</sup> Hualiang Jiang,<sup>‡</sup> Zhengming Li,<sup>§</sup> Zhen Liu,<sup>\*,†</sup> Weiliang Zhu,<sup>\*,‡</sup> and Jian-Guo Wang<sup>\*,§</sup>

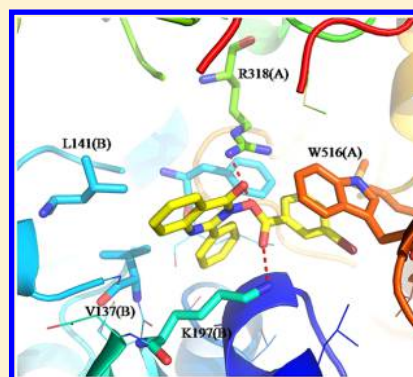
<sup>†</sup>Department of Clinical Laboratory, 309 Hospital of Chinese People's Liberation Army, Beijing 100091, China

<sup>‡</sup>State Key Laboratory of Drug Research, Drug Discovery and Design Center, Shanghai Institute of Materia Medica, Shanghai 201203, China

<sup>§</sup>State Key Laboratory and Institute of Elemento-Organic Chemistry, Nankai University, Tianjin 300071, China

## S Supporting Information

**ABSTRACT:** Acetohydroxyacid synthase (AHAS) has been regarded as a promising drug target against *Mycobacterium tuberculosis* (MTB) as it catalyzes the biosynthesis of branched-chain amino acids. In this study, 23 novel AHAS inhibitors were identified through molecular docking followed by similarity search. The determined IC<sub>50</sub> values range from 0.385 ± 0.026 μM to >200 μM against bacterium AHAS. Five of the identified compounds show significant in vitro activity against H37Rv strains (MICs in the range of 2.5–80 mg/L) and clinical MTB strains, including MDR and XDR isolates. More impressively, compounds 5 and 7 can enhance the killing ability against macrophages infected pathogen remarkably. This study suggests our discovered inhibitors can be further developed as novel anti-MTB therapeutics targeting AHAS.



## INTRODUCTION

Although *Mycobacterium tuberculosis* (MTB) is preventable and curable, this global infectious disease still remains one of the most terrible killers in the world. The emerged multidrug-resistant MTB (MDR-MTB) and extensively drug-resistant MTB (XDR-MTB) make this problem increasingly more complex for which little strategy has been confirmed to be effective.<sup>1</sup> In 2011, an estimated 220000–400000 cases of MDR-MTB emerged all over the world.<sup>2</sup> Among the global MTB cases, about 3.7% of new MTB patients have MDR-MTB strains and almost 60% of the MDR-MTB cases are estimated to occur in Brazil, China, India, the Russian Federation, and South Africa.<sup>2</sup> Respecting that the drug-resistant patterns are generally due to target gene mutation, it is urgently required to discover novel antimycobacterial compounds that work on distinctive targets and take effect by diverse mechanisms of action for the treatment of MDR-MTB and XDR-MTB infections.<sup>3,4</sup> However, although a number of lead compounds have been developed for new candidate drugs, no new chemical entity has really emerged for clinical use.

Acetohydroxyacid synthase (AHAS, EC 2.2.1.6, also referred as acetolactate synthase, ALS) used to be a biological target for “green herbicide” research,<sup>5–12</sup> and recently, it has been identified as an attractive target for design and development of new generation of anti-MTB agents.<sup>13,14</sup> AHAS catalyzes the first step in the branched-chain amino acids (leucine, isoleucine,

and valine) biosynthesis pathway,<sup>15</sup> which only occurs in higher plants, algae, fungi, and bacteria. Specific AHAS inhibitors show no or little mammalian toxicity because its homologous protein was not found in human and animals.<sup>16</sup> It has been discovered that sulfonylurea and imidazolinone (Figure 1) are effective inhibitors of plant AHAS, and they have already been used widely and safely as commercial herbicides for nearly 30 years.<sup>17,18</sup> As the binding pockets of AHAS from different sources (bacteria, fungi, or plants) share significant similarity (Figure S1, Supporting Information), plant AHAS inhibitors are predicted to also inhibit bacterium AHAS and consequently exhibit antimycobacterial activity against MTB strains. Indeed, some groups have investigated the bacteriostasis of sulfonylurea compounds such as sulfometuron methyl (SMM), chlorimuron methyl (CE), and metsulfuron methyl (MSM) against MTB-AHAS and MTB strains, proving their activity both in vitro and in vivo.<sup>13,19–21</sup>

Given the documented importance of AHAS in MTB, efforts have been made to discover new AHAS inhibitors as anti-MTB agents. Choi et al. reported some novel MTB-AHAS inhibitors through high throughput screening of a chemical library with 5600 compounds, and these compounds exhibited moderate anti-MTB activity.<sup>20</sup> Sohn et al. tested a number of sulfonylurea

Received: September 21, 2012

Published: January 14, 2013

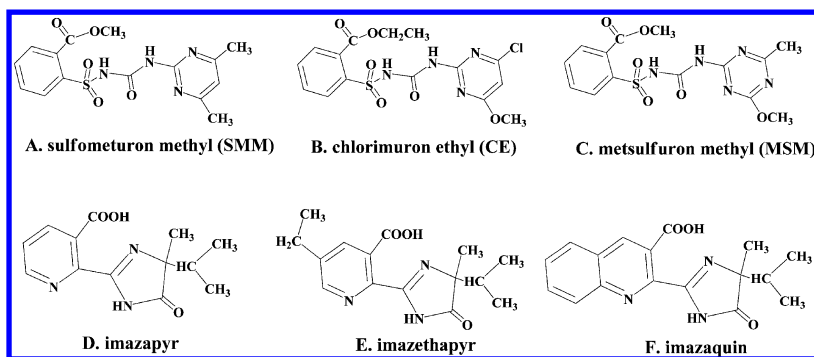


**Figure 1.** Structures of typical AHAS inhibitors. Sulfonylurea (A–C) and imidazolinone (D–E) herbicides.

derivatives, and some of them were found to possess efficacy against clinical MTB strains.<sup>19</sup> More recently, Wang and Li et al. reported that some monosubstituted sulfonylureas, of which the heterocyclic ring is substituted with only one substituent at the meta-position, also show visible activity against TB, including Chinese clinical MDR and XDR cases.<sup>22</sup> However, even the most potent reported sulfonylurea AHAS inhibitor, SMM, demonstrates much lower efficacy than the current MTB treatment regimen, and it does not act obviously in the ex vivo and in vivo anti-MTB assay. A previous mouse model study found that a high dose of 500 mg/kg daily of SMM is required to prevent the growth of MTB in the lung, suggesting that the activity is poor in the host.<sup>13</sup> Therefore, screening for more powerful AHAS inhibitors is required to develop new drugs. Herein, we report our efforts to further explore novel AHAS inhibitors via a structure-based virtual screening followed by bioassays, with the aim to identify more potent anti-MTB agents. The amino acid sequence similarity between *Escherichia coli* (*E. coli*)-AHAS II and MTB-AHAS is fairly high, suggesting that inhibitors may share similar activity against both the bacteria AHASs. Therefore, the compounds screened in silico were initially evaluated for inhibition of *E. coli*-AHAS II. In this work, a great number of hits were identified to show potent activity in the in vitro AHAS assay. Furthermore, several of them also display significant in vitro and intracellular activity against both standard and clinical MTB isolates, indicating that they may act as valuable starting points for the research of anti-MTB agents.

## RESULTS

### Homology Model Generation and Evaluation.

Although it is widely accepted that the active site of MTB-AHAS is formed by two catalytic subunits,<sup>23</sup> the three-dimensional (3D) crystal structure of MTB-AHAS is still unavailable until now. Therefore, homology modeling was adopted to build the 3D dimeric structure of MTB-AHAS based on the template protein (*Saccharomyces cerevisiae* AHAS, PDB code: 1N0H, referred to as yeast-AHAS in this paper).<sup>24</sup> The sequence alignment showed a 42% identity between MTB-AHAS and yeast-AHAS (Figure S2, Supporting Information), which is high enough for homology modeling.

Figure S3 of the Supporting Information shows that highly reliable models were obtained as all the amino acids for each model are in the allowed regions predicted by PROCHECK.<sup>25</sup> Another well-known program, namely, ProSA (Protein Structure Analysis),<sup>26</sup> was adopted to further check the quality of homology MTB-AHAS model. The Z-scores,<sup>26</sup> a parameter describing the overall model quality, were predicted to be

**Table 1.** Best *FitValue* and *Glidescore* of 21 Compounds That Belong to Two Different Groups

Compound name	<i>Glidescore</i>	<i>FitValue</i> <sup>c</sup>	Group
K12147 <sup>a</sup>	−7.73	2.88	active
K13030 <sup>a</sup>	−7.48	2.60	active
Promisulfuron methyl (PSM) <sup>b</sup>	−7.21	3.22	active
Chlorimuron ethyl (CE) <sup>b</sup>	−6.97	3.64	active
Sulfometuron methyl (SMM) <sup>b</sup>	−6.83	3.35	active
Chlorsulfuron (CS) <sup>b</sup>	−6.82	2.04	nonactive
KHG20613 <sup>b</sup>	−6.77	3.92	active
Pyrazosulfuron ethyl (PSE) <sup>b</sup>	−6.72	3.17	active
KHG20614 <sup>b</sup>	−6.59	2.01	active
Nicosulfuron (NS) <sup>b</sup>	−6.56	3.34	active
Metsulfuron methyl (MSM) <sup>b</sup>	−6.54	3.01	active
Triasulfuron (TS) <sup>b</sup>	−6.53	2.96	active
KHG20616 <sup>b</sup>	−6.36	1.71	active
KHG20612 <sup>b</sup>	−6.35	2.18	active
K13010 <sup>a</sup>	−6.21	2.16	active
Bensulfuron methyl (BSM) <sup>b</sup>	−6.18	—	nonactive
Thifensulfuron methyl (TSM) <sup>b</sup>	−5.76	—	nonactive
Imazapic <sup>b</sup>	−5.19	—	nonactive
Imazapyr <sup>b</sup>	−4.95	—	nonactive
Imazaquin <sup>b</sup>	−4.86	—	nonactive
Imazethapyr <sup>b</sup>	−4.22	—	nonactive

<sup>a</sup>Compounds collected from reference 19. <sup>b</sup>Compounds collected from reference 20. <sup>c</sup>Only the best *FitValue* for the compounds are given.

−11.18 and −10.48 for chain A and chain B of the MTB-AHAS structure model, respectively (Figure S4A, Supporting Information). Both values are within the range of Z-scores found for native proteins of similar size, indicating that the overall quality of our model is high. The energy plots (Figure S4B, Supporting Information) shows that only the loop (212–219 aa) in chain B has a moderate larger energy and can be directly viewed through C- $\alpha$  traces (Figure S4C, Supporting Information). However, this loop is far away from the binding site and will not affect our subsequent study.

**Docking Results of Active Ligands.** Twenty-one AHAS inhibitors were collected from the published literatures (Table S1, Supporting Information), 14 of which show different inhibition against the catalytic subunit of MTB-AHAS, while the rest do not exhibit such inhibitory activity.<sup>19,20</sup> Hence, these compounds were classified into two groups, “active” or “non-active” against MTB-AHAS. The docking results by Glide program are shown in Table 1. For each compound, five poses were saved initially, and eventually, one of the docked poses was retained mainly based on the *Glidescore* and the

**Table 2. Specific Feature Elements for Each Pharmacophore and Screening Results for Decoy Data Set**

Pharmacophore	RA <sup>a</sup>	HP <sup>a</sup>	HBA <sup>a</sup>	HBD <sup>a</sup>	Map_decoy (N/M) <sup>b</sup>
SMM.chm	2	3	3	0	0/1
CS.chm	2	3	3	0	2/3
K13010.chm	0	1	4	0	5/333
NS.chm	0	2	4	0	8/41
MSM.chm	0	1	4	0	4/128
KHG20616.chm	1	2	3	0	9/406
PSM.chm	0	4	2	0	5/259
TS.chm	1	3	1	0	9/600
KHG20612.chm	0	2	2	0	11/1960
KHG20613.chm	1	3	2	0	1/76
CE.chm	0	4	3	0	0/19
K13030.chm	1	2	4	0	0/3
KHG20614.chm	1	2	3	0	0/0
PSE.chm	2	2	3	0	—
K12147.chm	1	4	3	1	—

<sup>a</sup>Feature elements: ring aromatic (RA), hydrophobic (HP), hydrogen bond acceptor (HBA), and hydrogen bond donor (HBD). <sup>b</sup>M: number of compounds that can map to the corresponding pharmacophore. N: number of compounds from the 15 molecules among M.

hydrophobic, hydrogen bond and charge–charge interactions between this compound and the protein. According to the *Glidescore*, 14 active ligands were ranked ahead of the nonactive compounds except chlorsulfuron (CS), which demonstrated that the Glide program is suitable for inhibitor identification against MTB-AHAS. For every active ligand, a protein–ligand complex was formed between the selected docked pose of this ligand and the protein; thus, 14 protein–ligand complexes were created for pharmacophore analysis. Moreover, the nonactive compound CS had a higher *Glidescore* than the other nonactives; thus, the protein–CS complex was also created for further analysis.

**Pharmacophore Search.** Fifteen pharmacophore models were generated by *LigandScout* based on 15 ligand–protein

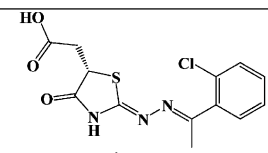
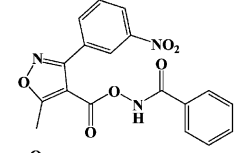
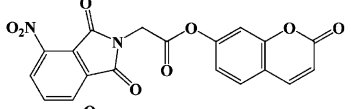
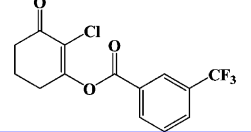
complexes obtained from docking (Table 2) with various feature elements including hydrophobic (HP), ring aromatic (RA), hydrogen bond acceptor (HBA), and hydrogen bond donor (HBD). The decoy data set tests revealed that different pharmacophore models have different performance. According to the result, 9 models (CS.chm, K13010.chm, NS.chm, MSM.chm, KHG20616.chm, PSM.chm, TS.chm, KHG20612.chm, and KHG20613.chm) were chosen for virtual screening. Table 1 lists the best *FitValue* for the 15 compounds. After pharmacophore screening, 30523 candidate compounds in total were obtained from the two databases (Specs and Maybridge databases with 197116 and 70626 compounds, respectively). All of the candidates were then docked to the catalytic subunits of MTB-AHAS model with the Glide program for further screening.

**Compound Selection.** The *Glidescore* of CE, a validated inhibitor of MTB-AHAS, was predicted to be  $-6.97$ ; thus,  $-7.00$  was set as a cutoff of *Glidescore* during the virtual screening. To evaluate the druglikeness of compounds with *Glidescore* smaller than  $-7.00$ , Lipinski's rule of five was used to filter out compounds with undesired features. However, the molecular weights of compounds were not strictly limited to 500. Then structure cluster analysis was adopted to achieve structural diverse compounds. Finally, the binding modes of the rest compounds were checked by visual observation to remove false-positive compounds. After all above-mentioned screening processes, a total of 95 compounds were purchased for bioassay.

Through in vitro enzyme assay, four hits (1, 2, 3, 4) exhibited inhibition activity against *E. coli*-AHAS II (Table 3). The most active agent was compound 4 with an  $IC_{50}$  value of  $2.67 \pm 0.11$   $\mu$ M, followed by 1 ( $IC_{50} = 11.58 \pm 2.05$   $\mu$ M), 2 ( $IC_{50} = 37.54 \pm 2.22$   $\mu$ M), and 3 ( $IC_{50} = 25.56 \pm 5.23$   $\mu$ M). SMM and CE were used as control compounds, and they showed the  $IC_{50}$  values of 0.58  $\mu$ M and 0.031  $\mu$ M, respectively.<sup>27</sup>

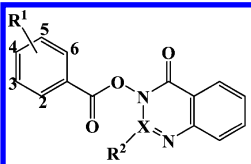
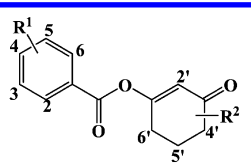
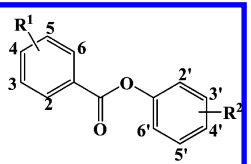
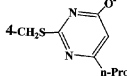
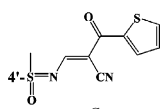
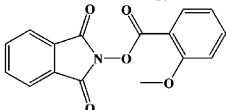
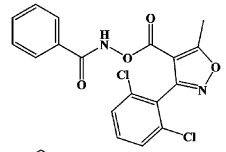
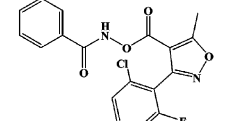
**Similarity Search.** A substructure similarity search was performed against the Specs and Maybridge databases based on the identified four novel inhibitors, which enabled us to retrieve

**Table 3. Biological Activity of First Screened AHAS Inhibitors**

Compound	Structure	Inhibition (%) <sup>a</sup>	$IC_{50}(\mu M)$ <sup>b</sup>	MIC (mg/L) <sup>c</sup>
1		90	$11.58 \pm 2.05$	>80
2		85	$37.54 \pm 2.22$	>80
3		90	$25.56 \pm 5.23$	>80
4		95	$2.67 \pm 0.11$	40

<sup>a</sup>Inhibition rate of compounds at 100 mg/L for *E. coli*-AHAS II. <sup>b</sup> $IC_{50}$  values of compounds against *E. coli*-AHAS II. <sup>c</sup>MIC of compounds for H37Rv.

Table 4. Structures and Biological Activity of Active analogs

<div style="display: flex; justify-content: space-around; align-items: center;"> <div style="text-align: center;">  <p>5-7</p> </div> <div style="text-align: center;">  <p>8-10</p> </div> <div style="text-align: center;">  <p>11-20</p> </div> </div>						
Compound	R <sup>1</sup>	R <sup>2</sup>	X	Inhibition (%) <sup>a</sup>	IC <sub>50</sub> (μM) <sup>b</sup>	MIC (mg/L) <sup>c</sup>
5	3-Br	Ph	C	100	1.85 ± 0.19	2.5
6	4-NO <sub>2</sub>	-	N	97	14.13 ± 3.27	20
7	3-CF <sub>3</sub>	Ph	C	97	2.02 ± 0.15	2.5
8	4-Cl	4'-COOCH <sub>3</sub> , 5'-(CH <sub>3</sub> ) <sub>2</sub>	-	99	24.21 ± 1.52	80
9	2-Cl	2'-Cl	-	100	1.78 ± 0.09	80
10	4-Cl	5'-(CH <sub>3</sub> ) <sub>2</sub>	-	98	14.1 ± 1.4	10
11	3-CF <sub>3</sub>	2', 4'-Cl, 6'-COCH <sub>3</sub>	-	75	> 200	40
12	3-CF <sub>3</sub>	2'-NO <sub>2</sub> , 4'-CF <sub>3</sub>	-	98	17.43 ± 2.12	40
13	2,4-Cl	2'-NO <sub>2</sub> , 4'-CF <sub>3</sub>	-	99	13.89 ± 2.14	> 80
14	3-Cl	2'-NO <sub>2</sub> , 4'-CF <sub>3</sub>	-	99	17.09 ± 2.52	80
15	4-Cl	2'-NO <sub>2</sub> , 5'-SO <sub>2</sub> Ph	-	100	0.385 ± 0.026	5
16		2', 4'-F	-	81	> 200	> 80
17	4-CH <sub>3</sub>	2'-N-morpholino	-	96	152.2 ± 39.9	ND <sup>d</sup>
18	-	2'-COCH=CHCO-3'	-	71	> 200	> 80
19	4-Cl		-	61	> 200	40
20	3,5-CF <sub>3</sub>	4'-thiazole	-	72	> 200	40
21				99	19.65 ± 2.97	80
22				93	87.28 ± 17.29	80
23				96	28.72 ± 4.28	ND <sup>d</sup>

<sup>a</sup>Inhibition rate of compounds at 100 mg/L for *E. coli*-AHAS II. <sup>b</sup>IC<sub>50</sub> values of compounds against *E. coli*-AHAS II. <sup>c</sup>MICs of compounds for H37Rv. <sup>d</sup>ND: not determined.

1038 compounds. These compounds were clustered and visually checked for filtering, and finally, 108 compounds were selected for in vitro enzyme assays. Herein, 19 compounds with observed activity against bacterium AHAS were identified (Table 4). The most potent hit is **15**, with IC<sub>50</sub> value of 0.385 ± 0.026 μM, followed by **9** (1.78 ± 0.09 μM), **5** (1.85 ± 0.19 μM), and **7** (2.02 ± 0.15 μM). The ESI-MS or HRMS data of representative compound **4**, **7**, and **15** are shown in Figure S5 of the Supporting Information.

**Measurement of in Vitro Antimycobacterial Activity against MTB.** The active compounds were subsequently tested for their efficacy against standard MTB strain H37Rv (Table 3 and 4). The MICs of **5** and **7** against H37Rv are 2.5 mg/L, and **15** exhibits an MIC of 5 mg/L. These three compounds are 2–3 fold more active than the control SMM and are compared favorably with some known anti-MTB agents. Compound **10** displays an equal MIC value with SMM (10 mg/L). Compounds **6**, **8**, **11**, **12**, **14**, **22**, **19**, **21**, **20**, and **4** possess MIC values at the range of 20–80 mg/L.



**Table 5. Antimycobacterial Activity of Compounds against Clinical Isolates of MTB<sup>a</sup>**

No. of isolates	Isolates	Resistance phenotype	MIC(mg/L)				
			5	7	15	10	4
A	H37Rv	susceptible	2.5	2.5	5	10	40
	All-susceptible	susceptible	2.5	2.5	5	10	80
B	Single-resistant	INH	2.5	2.5	5	10	40
C	Single-resistant	INH	2.5	2.5	5	10	40
D	MDR	RFP, INH	2.5	2.5	5	10	40
E	MDR	RFP, INH, SM	2.5	2.5	5	10	40
F	MDR	RFP, INH, EMB	2.5	2.5	5	10	40
G	MDR	RFP, INH, EMB	2.5	2.5	5	10	40
H	XDR	RFP, INH, AM, OLF	2.5	2.5	5	10	40
I	XDR	RFP, INH, KN, OLF	2.5	2.5	5	10	80
J	XDR	RFP, INH, AM, OLF	2.5	2.5	5	10	40

<sup>a</sup>RFP, rifampin; INH, isoniazid; SM, streptomycin; EMB, ethambutol; OLF, ofloxacin; KN, kanamycin; AM, amikacin.

In addition, efficacy of **4**, **5**, **7**, **10**, and **15** against 10 clinical MTB strains isolated from the Chinese People's Liberation Army (PLA) 309 hospital<sup>28</sup> were further determined (Table 5). As expected, they exhibited equivalent or comparative activity against MDR and XDR isolates compared with that against the susceptible strains.

In order to determine whether the identified compounds inhibit the growth of tuberculosis targeting AHAS, we compared the activity of the most potent agents, **5** and **7**, in the medium with or without additional branched-chain amino acids (leucine, isoleucine, and valine).<sup>29</sup> Interestingly, we found that they did not show any inhibition at the MIC when branched-chain amino acids were added (data not shown), which confirmed their sterilization mechanism targeting AHAS.

**Measurement of Intracellular Antimycobacterial Activity against MTB.** THP-1 macrophages were infected with H37Rv and clinical MDR/XDR isolates (E, J), and then exposed to **5** and **7** for 96 h. The presence of **5** and **7** caused a dose dependent inhibition against intracellular MTB isolates (Figure 2). Both the compounds can kill more than 80% pathogens at 40 mg/L, regardless of their drug resistant phenotype, and are found to be nontoxic at this concentration. TNF-alpha of every supernatant was determined by enzyme-linked immunosorbent assay (ELISA) simultaneously, and concordant decrease was also observed (Figure 3).

## DISCUSSION

Combination of no less than four effective drugs is recommended to treat tuberculosis. However, MDR and XDR cases have increased the difficulty of the treatment, leading to higher cost and a longer treatment cycle. Especially, XDR-MTB combining with HIV infection caused a high rate of death every year.<sup>1,2</sup> Hardly any treatment strategy was considered effective for these strains. Therefore, the discovery of new anti-MTB drugs is urgently needed.

Recent molecular mechanism studies of AHAS in tuberculosis indicated that AHAS could be considered as a potential

target for antimicrobial drug development.<sup>14,30,31</sup> Although several types of novel AHAS inhibitors have been recently identified, to the best of our knowledge, this is the very first report to discover new anti-MTB agents through virtual screening targeting this enzyme. In this study, we successfully discovered several novel structural AHAS inhibitors and evaluated their antimicrobial activity against MTB. From the initial screening, only one compound, **4**, was confirmed to be a real anti-MTB agent. As shown in Figure 4, the binding site of **4** is located at the dimer interface involved in residues from both chains. LigPlot program was adopted to automatically explore the protein–ligand interactions (Figure 4A).<sup>32</sup> Three oxygen atoms in **4** form hydrogen bonds with amino acids R318(A), G138(B), and K197(B), respectively, leading to a strong binding affinity between this compound and the protein. Furthermore, the 3-trifluoromethyl benzene fragment is surrounded by the hydrophobic amino acids such as M512(A), W516(A), G62(B), and F147(B) and thus forms extensive hydrophobic interactions with the protein. In addition to hydrogen bonding and hydrophobic interactions, the  $\pi$ – $\pi$  stacking interaction between the benzene ring and W516(A) is of critical importance to the binding of this compound to MTB-AHAS (Figure 4B). As shown in Figure 4C, in the crystal structure of the yeast-AHAS/CE complex, four hydrogen bonds are formed between the ligand and the protein via the residue R380. Compared to this, three hydrogen bonds are generated between **4** and R318, G138, and K197 in MTB-AHAS. The corresponding arginine also played an important role in herbicides bound to plant AHAS (R377). In addition, the  $\pi$ – $\pi$  stacking interaction between the aromatic ring and W516 (W586 in yeast-AHAS) is also conserved between different AHASs, indicating the similar binding modes between CE and **4**.

The substructure similarity search afforded us 19 active compounds against AHAS, all of which bind to the active site and retain key interactions with the protein as the original compounds. Here, we mainly discuss the structure–activity relationships of compound **4** analogs. They are benzoate derivatives and can be divided into three groups based on the different substituents. The most potent group includes **5**, **6**, and **7**, and the MIC for H37Rv of them is 2–16 times lower than that of **4**. However, **5** is more potent than **6** in the antimycobacterial activity measurement experiment, indicating their different binding details. Compared to **6**, the 2-phenyl substituted quinazolinone in **5** (Figure 5A) occupies a small hydrophobic pocket, which increases its inhibition activity. Moreover, the nitrobenzene in **6** cannot match well with the aromatic ring of W516 (Figure 5B), resulting a weaker  $\pi$ – $\pi$  stacking interaction than **5**, which also attenuates the activity of **6**.

The second group consists of **8**, **9**, and **10**, and their structures are very similar to **4**. However, these three compounds show different antimycobacterial activity against MTB in vitro. For example, the MIC for H37Rv of **8** is eight times higher than that of **10**, which is due to the methoxycarbonyl substituent of **8**. This large substitutional group is the reason that **8** cannot embed into the in-depth pocket like **10**, thus weakening its anti-MTB activity compared to **10** (Figure 5C,D). It is puzzling that **9** displayed high activity against AHAS but low efficacy against MTB. This result may be due to the poor penetration of **9** into cells.

The rest of the analogs belong to the third group, and their activities in vitro are less potent than **4**, except for compound

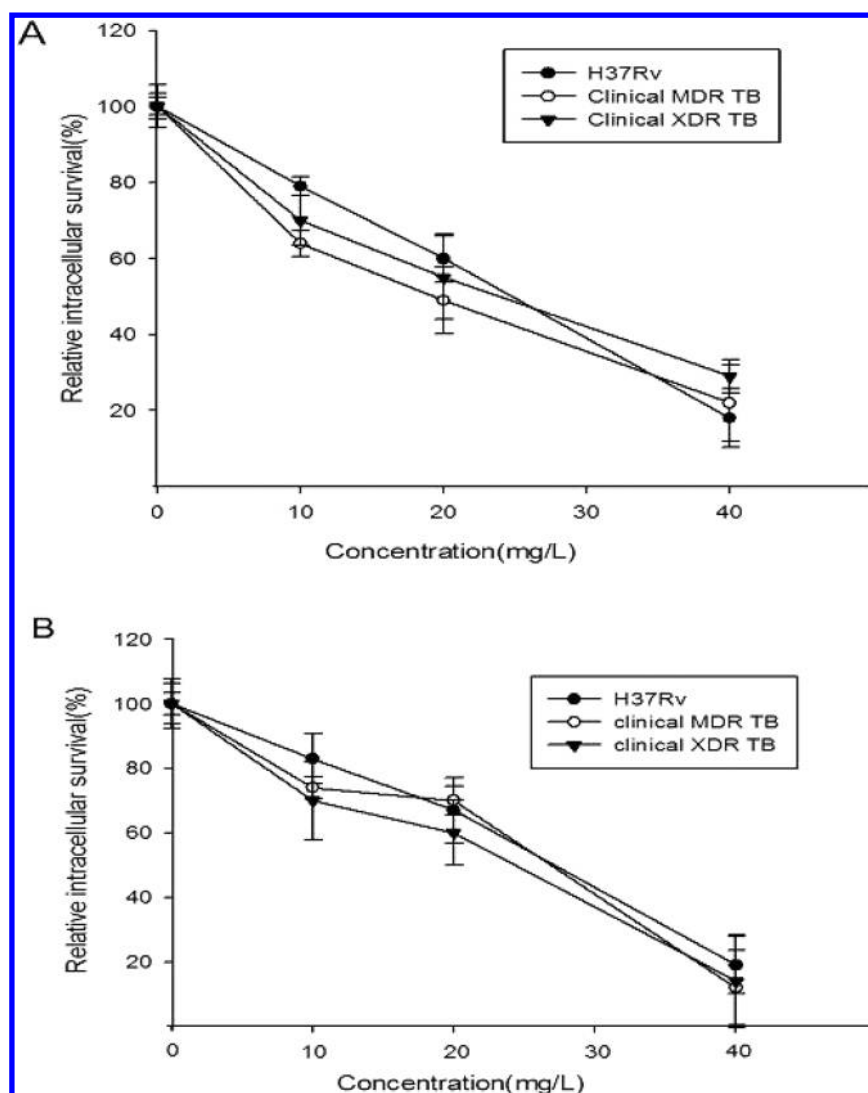


**Figure 2.** Capacity of **5** (A) and **7** (B) to inhibit the growth of MTB within THP-1 macrophages.

**15.** We selected two compounds (**14** and **15**) to study the reason for the big difference of their inhibition activities. Compared with the para-trifluoromethyl substituent in **14** (Figure 5E), the meta-phenylsulfonyl group in **15** (Figure 5F) extends into an additional hydrophobic pocket which locates at the MTB-AHAS dimer interface, leading to the anti-MTB activity greatly increasing.

Although hundreds of compounds have activity in vitro against TB strains, very few of them are efficient where the macrophage resides in the mammalian lung. However, assessment of their in vivo activity is costly and time consuming. Therefore, it is of far greater significance to test their capability of killing intracellular MTB in human macrophage. Considering that compounds **5** and **7** are significantly effective against MTB in the THP-1 macrophages, therapeutic effects of them in vivo are expected. TNF- $\alpha$  is a pleiotropic cytokine, and its role in harmful or beneficial inflammatory processes is complex. Up-regulation of TNF- $\alpha$  plays an important role in the inflammatory response to MTB infection. Here, we can see that TNF- $\alpha$  expression is blocked by the compounds in infected macrophages but not in control macrophages, indicating that the compounds can eliminate inflammation by killing MTB.

Another important point of this work is that we have evaluated the antimicrobial activity of inhibitors against clinical MTB strains isolated from the PLA 309 hospital in China, including MDR and XDR cases. As we know, activity of drugs against MTB always vary markedly among different areas, and there may be cross resistance on two antibiotics. Here, we found that new identified compounds are very effective against all the clinical strains isolated from the PLA 309 hospital of China, and no obvious difference is shown among drug-susceptible strains and drug-resistant strains, suggesting that these compounds may be promising lead structures for the development of novel anti-MTB therapeutics in China. Current studies are ongoing to design a new series based on these structures to find more efficacy anti-MTB agents in our laboratory, and evaluation of the in vivo efficacy will be performed in the near future.

## ■ EXPERIMENTAL SECTION

**Amino Acid Sequence Alignment and Homology Modeling.** The amino acid sequence of MTB-AHAS, retrieved from UniProt database (accession number P0A622) was aligned with that of yeast-AHAS (accession number P07342) using the program Clustal W.<sup>33</sup> For the template structure, all

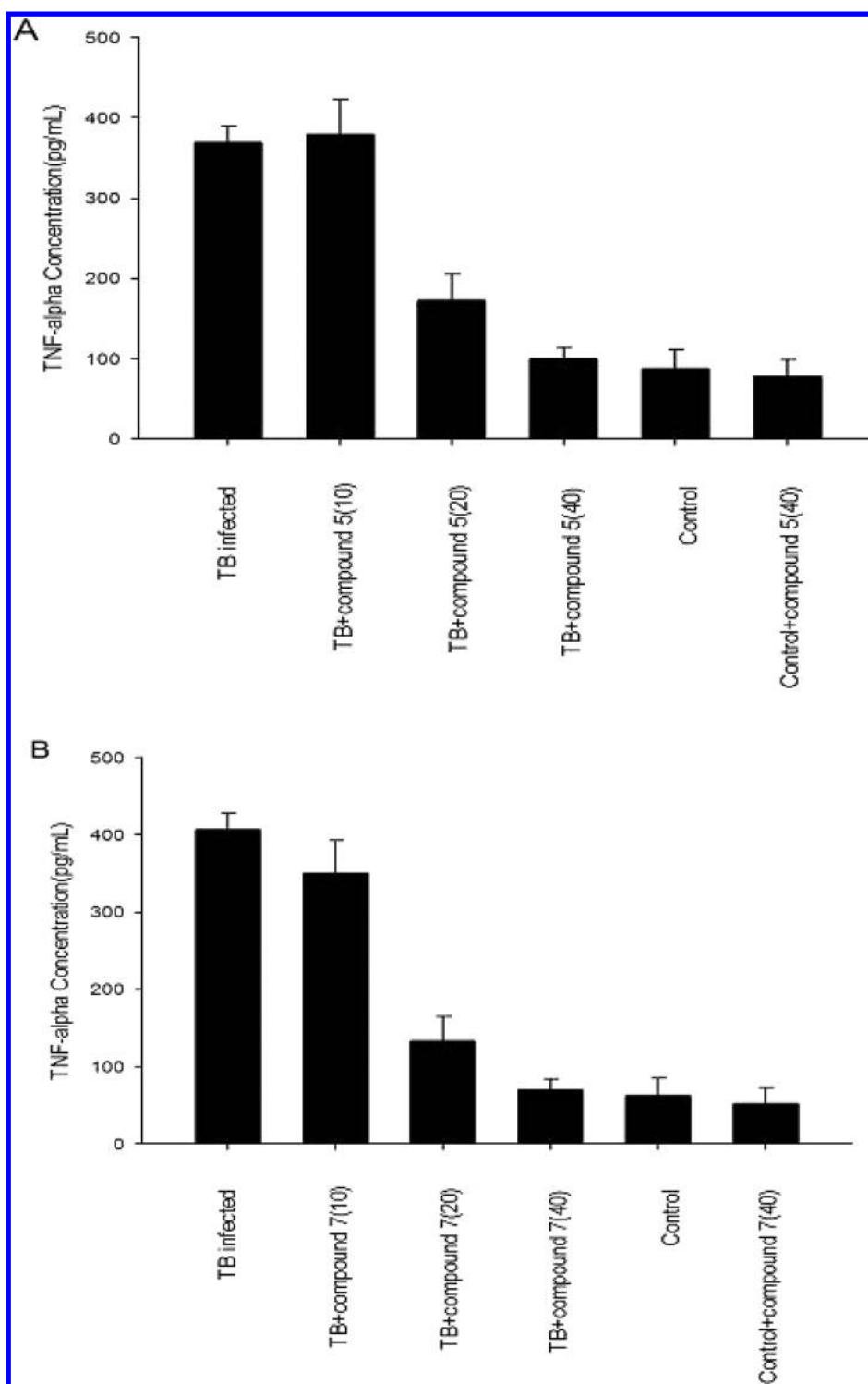


**Figure 3.** Capacity of 5 (A) and 7 (B) to block the up-regulation of TNF- $\alpha$  caused by MTB infection within THP-1 macrophages.

the waters, ligands, and three cofactors were removed to model the 3D dimeric structure of MTB-AHAS.

Homology modeling of the catalytic subunits of MTB-AHAS was carried out using the HOMOLGY module within Insight II.<sup>34</sup> Two chains of the dimer were built and optimized. For each chain, after a simple optimization with Insight II, energy minimization was then accomplished through the following steps with SYBYL 6.8 using AMBER force field.<sup>35,36</sup> First, all the heavy atoms of the primary models were fixed to optimize hydrogen atoms only. Second, all the backbone atoms were

fixed to optimize the side-chain atoms. Third, all the atoms were fully optimized. One of the cofactors,  $Mg^{2+}$ , is found in the template protein through coordination bonds with D550, N577, and E579 (D480, N507, and N509 numbered by MTB-AHAS), respectively, so all the minimization processes must be restricted in the same constraint of aggregating all heavy atoms of these three amino acids of MTB-AHAS to ensure the stereo configuration of coordination bonds. The dimeric model of the MTB-AHAS catalytic subunits was constructed through the combination of the two chains directly and the same energy



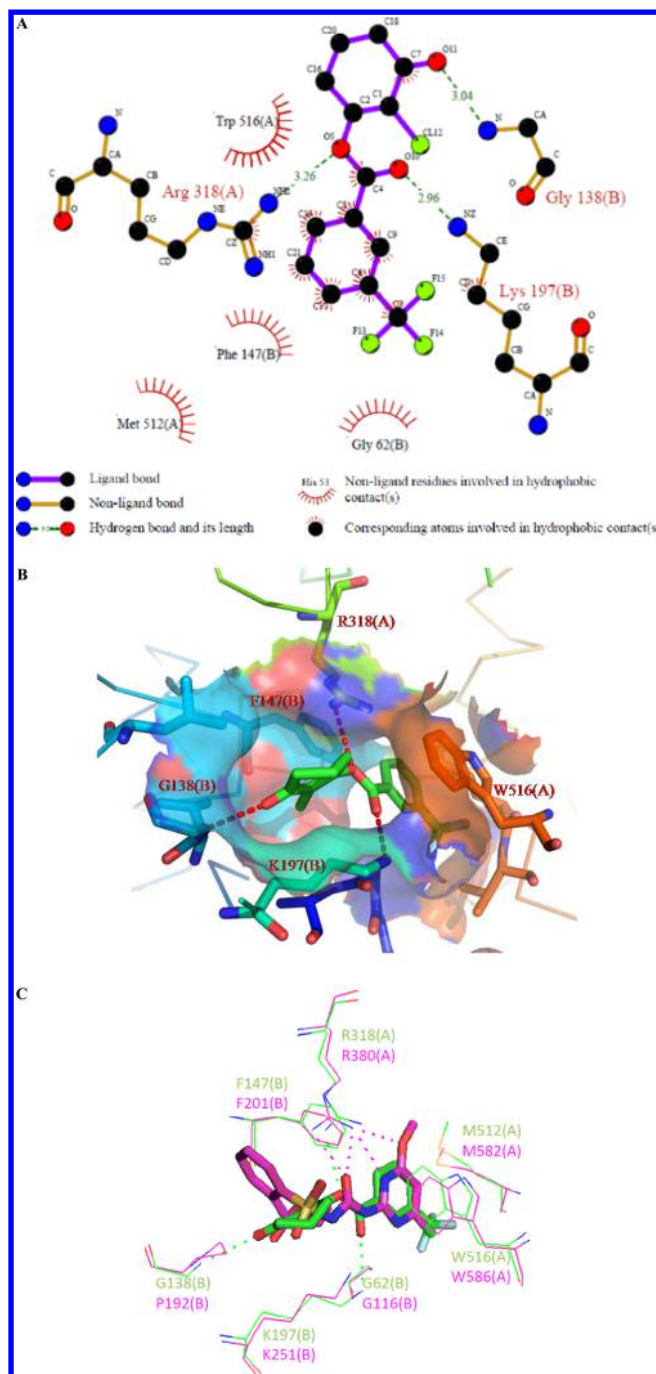


**Figure 4.** Binding mode of **4** in the active pocket of MTB-AHAS. (A) Hydrogen bonds and hydrophobic interactions between **4** and MTB-AHAS by LigPlot program. Corresponding residue numbers are given in parentheses. (B) Stereo diagram of **4** with MTB-AHAS in which **4** is showed in green sticks. The binding pocket of MTB-AHAS is displayed as a transparent surface, and the residues involved in hydrogen bonding (red dashed line) and hydrophobic interaction are shown in stick mode as well. (C) Comparison of binding mode between CE and **4**. Ligands are displayed in stick mode, and hydrogen bonds are shown in dashed lines. CE is bound to yeast-AHAS (PDB code: 1N0H) with carbon atoms colored magenta, and only the key involved residues are shown in lines labeled with magenta. The complex of MTB-AHAS and **4** is colored in green and displayed in the same mode as above. This figure was done with PyMOL.<sup>43</sup>

minimization procedure for the model optimization was performed in SYBYL 6.8. Finally, the coordinates of ligand

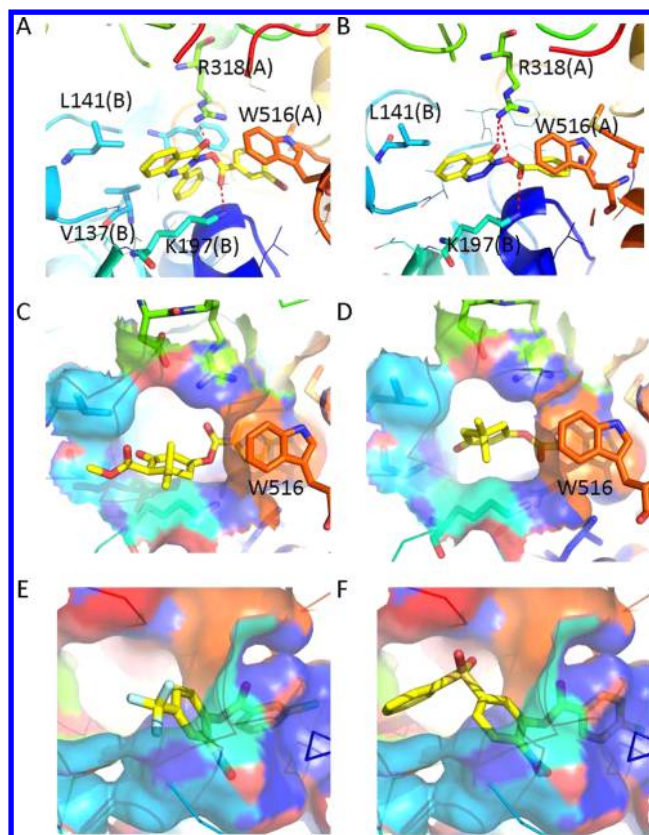


**Figure 5.** Binding mode analysis of active analogs with MTB-AHAS. Detailed interactions of **5** (A) and **6** (B) with surrounding key residues were analyzed. Compounds are shown in yellow sticks, while surrounding key residues from different chains are shown in chromatic sticks. Compound **8** (C), **10** (D), **14** (E), and **15** (F) within the active pocket are shown in the stereo diagrams in which active compounds are shown in yellow sticks, and the pocket is displayed as a transparent surface.

and cofactors were directly derived from the crystal structure of yeast-AHAS by simple structural alignment. The generated model was then validated by PROCHECK and ProSA program.

**Molecular Docking.** The docking was performed using the Glide program (grid-based ligand docking with energetics) in the Schrödinger suite of software. During the homology modeling, the coordinates of the ligand were added to the homology model from the crystal structure of yeast-AHAS by simple structural alignment. Glide uses the position and size of the aligned ligand to determine the region for which grids will be generated, representing the binding site of the receptor. The default center of this region is the centroid of the ligand, and the default size was defined similar to the ligand, named the enclosing box. In docking screening using these receptor grids, ligands were confined to the enclosing box. Compounds were then docked to the protein in standard precision (SP) mode, with up to five poses saved per compound and other default parameters.

**Pharmacophore Generation and Validation.** *LigandScout*, a powerful 3D pharmacophore model generator on the basis of protein–ligand complex,<sup>37</sup> was employed in this work. Fifteen pharmacophore models were generated based on the protein–ligand complexes obtained from docking. Then, a decoy data set, which was consisted of 15 ligands (14 known active ligands of MTB-AHAS and chlorsulfuron, an known herbicide) and 10000 structural diverse molecules obtained



from DUD (Directory of Useful Decoys)<sup>38</sup> by Discovery Studio 2.1,<sup>39</sup> was used to validate the reliability of developed pharmacophore models. The pharmacophore models with good performance were used as 3D queries to search database.

**Pharmacophore-Based Virtual Screening.** On the basis of the selected pharmacophore models, Specs (<http://www.specs.net/>) and Maybridge (<http://www.maybridge.com/>), compounds were mapped to each pharmacophore through the protocol *ligand pharmacophore mapping* in Discovery Studio 2.1, followed by molecular docking using Glide program. After the pharmacophore mapping was finished, the property of *FitValue*, a standard to measure how well a compound fits the pharmacophore, was given.<sup>40</sup> A higher *FitValue* represents a better fit. The candidate compounds were selected based on both the *FitValue* and *Glidescore*. Only the compounds that met the two kinds of criteria were then manually checked for sample preparation.

**In Vitro AHAS Inhibition.** The *E.coli*-AHAS isoenzyme II was expressed and purified as described previously.<sup>24,41</sup> The enzyme composes of both the catalytic and regulatory subunits. AHAS activity was measured using the colorimetric assay in 50 mM potassium phosphate (pH 7.0) containing 50 mM pyruvate, 1 mM thiamine diphosphate (ThDP), 10 mM MgCl<sub>2</sub>, and 10 μM flavin adenine dinucleotide (FAD). All compounds were originally dissolved in dimethyl sulfoxide (DMSO) at 50 mg/mL and then diluted by distilled water at certain concentration into the reaction mixture. The reaction mixture was incubated at 37 °C for 30 min, and the reaction was stopped with 25 μL of 10% H<sub>2</sub>SO<sub>4</sub> and heated at 60 °C for 15 min to convert acetolactate into acetoin. The formed acetoin was quantified by incubation with 0.5% creatine and α-naphthol (5%, w/v) for another 15 min at 60 °C, and A<sub>525</sub> was measured. The IC<sub>50</sub> values were calculated using the following equation<sup>42</sup>

$$v = v_0 / (1 + [I] / IC_{50})$$

**Measurement of Antimycobacterial Activity against MTB.** Standard MTB strain H37Rv (ATCC 27294), which is susceptible to all the anti-MTB drugs, was purchased from Beijing Institute for Tuberculosis Control. Ten clinical isolates, which were identified and characterized for their susceptibility to the first line and second line antibiotics by our team from the PLA 309 hospital,<sup>28</sup> were randomly selected in this work and numbered from A to J. All the isolates were cultured by Lowenstein–Jensen (LJ) medium before used.

Compounds were diluted 2-fold on Middlebrook 7H10 agar media supplemented with OADC (oleic acid, albumin, dextrose, and catalase). MTB strains were harvested from the LJ medium and collected by the solution with 0.05% tween-80. Each prepared MTB strain was added to each medicated media. The mediums were incubated at 36.5 °C, and the examination for bacterial growth was recorded four weeks later. Minimum inhibitory concentration (MIC) was defined as the lowest concentration of a compound that will inhibit the visible bacterial growth of MTB strains after incubation.

**Intracellular Activity Assay.** The 3-[4,5-dimethylthiazol-2-yl]-2,5-diphenyl tetrazolium bromide (MTT) assay was used to test the cytotoxicity of the active compounds in THP-1 cells according to previous description.<sup>22</sup> Subsequently, the intracellular activity assay was performed as follows: The THP-1 cells were distributed to the wells of a 12-well plate and were incubated in RPMI 1640 medium plus 10% fetal bovine serum (FBS) and 1% L-glutamine. The cells were differentiated into macrophages using 5 nM Phorbol myristate acetate (PMA).

After three days, three washes were performed with RPMI medium to remove all the non-adhered cells. Then new medium without PMA was added, and the cells were subsequently incubated for another two days. Differentiated THP-1 cells were infected with TB for 4 h at a ratio of 10 colony-forming unit (CFU) per macrophage. Infected THP-1 cells were then washed three times with RPMI to remove all the non-phagocytosed bacteria. Cells were treated with each tested compounds in RPMI medium. The medium without the compound was used as a negative control. After 4 days, the supernatant was used to test TNF-α by ELISA (TNF-α ELISA Kit, BOSTER Company, China). Meanwhile, infected cells were lysed with 0.1% Triton-X 100, and CFU counts of the cell lysates were determined by real-time polymerase chain reaction (PCR, *Mycobacterium tuberculosis* Real Time PCR Kit, Lifeliver Company, China).

## ■ ASSOCIATED CONTENT

### ● Supporting Information

Figures S1 to S5 and Table S1. This material is available free of charge via the Internet at <http://pubs.acs.org>.

## ■ AUTHOR INFORMATION

### Corresponding Author

\* E-mail: (Z. L.) [sensory@163.com](mailto:sensory@163.com); (W.Z.) [wzhu@mail.shcnc.ac.cn](mailto:wzhu@mail.shcnc.ac.cn); (J.-G.W.) [nkwjg@nankai.edu.cn](mailto:nkwjg@nankai.edu.cn). Tel: (Z. L.) +86-10-51520725; (W. Z.) +86-21-50805020; (J.-G.W.) +86-22-23499414. Fax: (W.Z.) +86-21-50805020; (J.-G.W.) +86-22-23503627.

### Author Contributions

<sup>||</sup>These authors contributed equally.

### Notes

The authors declare no competing financial interest.

## ■ ACKNOWLEDGMENTS

This work was financially supported by the National Natural Science Foundation of China (No. 81271777, No. 30970419, No. 81273435, and No. 81000001), National Basic Research Project of China (No. 2013CB734004 and No. 2010CB126103), National Key Technology Research and Development Program (No. 2011BAE06B05-3), and the International Collaboration Project from the S&T Ministry of China on drug and diagnostics innovation of tropical diseases (No. 2010DFA33970).

## ■ ABBREVIATIONS

AHAS, acetohydroxyacid synthase; ALS, acetolactate synthase; MTB, *Mycobacterium tuberculosis*; MIC, minimum inhibitory concentration; MDR, multidrug-resistant; XDR, extensively drug-resistant; SMM, sulfometuron methyl; CE, chlorimuron methyl; MSM, metsulfuron methyl; CS, chlorsulfuron; ThDP, thiamine diphosphate; FAD, flavin adenine dinucleotide; DMSO, dimethyl sulfoxide; PCR, polymerase chain reaction; ELISA, enzyme-linked immunosorbent assay; PMA, phorbol myristate acetate; CFU, colony-forming unit; FBS, fetal bovine serum; HP, hydrophobic; RA, ring aromatic; HBA, hydrogen bond acceptor; HBD, hydrogen bond donor; PLA, People's Liberation Army; RFP, rifampin; INH, isoniazid; SM, streptomycin; EMB, ethambutol; OLF, ofloxacin; KN, kanamycin; AM, amikacin; ProSA, protein structure analysis; MTT, 3-[4,5-dimethylthiazol-2-yl]-2,5-diphenyl tetrazolium bromide; 3D, three-dimensional

## REFERENCES

- (1) Global Tuberculosis Report 2012, World Health Organization. [http://apps.who.int/iris/bitstream/10665/75938/1/9789241564502\\_eng.pdf](http://apps.who.int/iris/bitstream/10665/75938/1/9789241564502_eng.pdf) (accessed January 22, 2013).
- (2) Multidrug-Resistant Tuberculosis (MDR-TB), 2012 Update, World Health Organization. <http://www.who.int/tb/publications/MDRFactSheet2012.pdf> (accessed January 22, 2013).
- (3) Koul, A.; Arnoult, E.; Lounis, N.; Guillemont, J.; Andries, K. The challenge of new drug discovery for tuberculosis. *Nature* **2011**, *469*, 483–490.
- (4) Sacks, L. V.; Behrman, R. E. Developing new drugs for the treatment of drug-resistant tuberculosis: a regulatory perspective. *Tuberculosis* **2008**, *88*, S93–100.
- (5) Chen, C. N.; Chen, Q.; Liu, Y. C.; Zhu, X. L.; Niu, C. W.; Xi, Z.; Yang, G. F. Syntheses and herbicidal activity of new triazolopyrimidine-2-sulfonamides as acetohydroxyacid synthase inhibitor. *Bioorg. Med. Chem.* **2010**, *18*, 4897–4904.
- (6) Xiong, Y.; Liu, J.; Yang, G. F.; Zhan, C. G. Computational determination of fundamental pathway and activation barriers for acetohydroxyacid synthase-catalyzed condensation reactions of alpha-keto acids. *J. Comput. Chem.* **2010**, *31*, 1592–1602.
- (7) Chen, C. N.; Lv, L. L.; Ji, F. Q.; Chen, Q.; Xu, H.; Niu, C. W.; Xi, Z.; Yang, G. F. Design and synthesis of N-2,6-difluorophenyl-5-methoxy-1,2,4-triazolo[1,5-a]-pyrimidine-2-sulfonamide as acetohydroxyacid synthase inhibitor. *Bioorg. Med. Chem.* **2009**, *17*, 3011–3017.
- (8) Ji, F. Q.; Niu, C. W.; Chen, C. N.; Chen, Q.; Yang, G. F.; Xi, Z.; Zhan, C. G. Computational design and discovery of conformationally flexible inhibitors of acetohydroxyacid synthase to overcome drug resistance associated with the W586L mutation. *ChemMedChem* **2008**, *3*, 1203–1206.
- (9) He, Y. Z.; Li, Y. X.; Zhu, X. L.; Xi, Z.; Niu, C.; Wan, J.; Zhang, L.; Yang, G. F. Rational design based on bioactive conformation analysis of pyrimidinylbenzoates as acetohydroxyacid synthase inhibitors by integrating molecular docking, CoMFA, CoMSIA, and DFT calculations. *J. Chem. Inf. Model.* **2007**, *47*, 2335–2244.
- (10) Li, Y. X.; Luo, Y. P.; Xi, Z.; Niu, C.; He, Y. Z.; Yang, G. F. Design and syntheses of novel phthalazin-1(2H)-one derivatives as acetohydroxyacid synthase inhibitors. *J. Agric. Food Chem.* **2006**, *54*, 9135–9139.
- (11) Xi, Z.; Yu, Z.; Niu, C.; Ban, S.; Yang, G. Development of a general quantum-chemical descriptor for steric effects: Density functional theory based QSAR study of herbicidal sulfonylurea analogues. *J. Comput. Chem.* **2006**, *27*, 1571–1576.
- (12) Yang, G.; Liu, H.; Yang, H. QSAR and 3D-QSAR analysis of structurally diverse ALS inhibitors: Sulfonylureas and triazolopyrimidine-2-sulfonamides. *Pestic. Sci.* **1999**, *55*, 1143–1150.
- (13) Grandoni, J. A.; Marta, P. T.; Schloss, J. V. Inhibitors of branched-chain amino acid biosynthesis as potential antituberculosis agents. *J. Antimicrob. Chemother.* **1998**, *42*, 475–482.
- (14) Singh, V.; Chandra, D.; Srivastava, B. S.; Srivastava, R. Biochemical and transcription analysis of acetohydroxyacid synthase isoforms in *Mycobacterium tuberculosis* identifies these enzymes as potential targets for drug development. *Microbiology* **2011**, *157*, 29–37.
- (15) Chipman, D.; Barak, Z.; Schloss, J. V. Biosynthesis of 2-aceto-2-hydroxy acids: Acetolactate synthases and acetohydroxyacid synthases. *Biochim. Biophys. Acta* **1998**, *1385*, 401–419.
- (16) Duggleby, R. G.; Pang, S. S. Acetohydroxyacid synthase. *J. Biochem. Mol. Biol.* **2000**, *33*, 1–36.
- (17) Chaleff, R. S.; Mauvais, C. J. Acetolactate synthase is the site of action of two sulfonylurea herbicides in higher plants. *Science* **1984**, *224*, 1443–1445.
- (18) Shaner, D. L.; Anderson, P. C.; Stidham, M. A. Imidazolinones: potent inhibitors of acetohydroxyacid synthase. *Plant Physiol.* **1984**, *76*, 545–546.
- (19) Sohn, H.; Lee, K. S.; Ko, Y. K.; Ryu, J. W.; Woo, J. C.; Koo, D. W.; Shin, S. J.; Ahn, S. J.; Shin, A. R.; Song, C. H.; Jo, E. K.; Park, J. K.; Kim, H. J. In vitro and ex vivo activity of new derivatives of acetohydroxyacid synthase inhibitors against *Mycobacterium tuberculosis* and non-tuberculous mycobacteria. *Int. J. Antimicrob. Agents* **2008**, *31*, 567–571.
- (20) Choi, K. J.; Yu, Y. G.; Hahn, H. G.; Choi, J. D.; Yoon, M. Y. Characterization of acetohydroxyacid synthase from *Mycobacterium tuberculosis* and the identification of its new inhibitor from the screening of a chemical library. *FEBS Lett.* **2005**, *579*, 4903–4910.
- (21) Zohar, Y.; Einav, M.; Chipman, D. M.; Barak, Z. Acetohydroxyacid synthase from *Mycobacterium avium* and its inhibition by sulfonylureas and imidazolinones. *Biochim. Biophys. Acta* **2003**, *1649*, 97–105.
- (22) Pan, L.; Jiang, Y.; Liu, Z.; Liu, X. H.; Wang, G.; Li, Z. M.; Wang, D. Synthesis and evaluation of novel monosubstituted sulfonylurea derivatives as antituberculosis agents. *Eur. J. Med. Chem.* **2012**, *50*, 18–26.
- (23) Souza, T. C. S.; Josa, D.; Ramalho, T. C.; Caetano, M. S.; da Cunha, E. F. F. Molecular modelling of *Mycobacterium tuberculosis* acetolactate synthase catalytic subunit and its molecular docking study with inhibitors. *Mol. Simulat.* **2008**, *34*, 707–713.
- (24) Pang, S. S.; Guddat, L. W.; Duggleby, R. G. Molecular basis of sulfonylurea herbicide inhibition of acetohydroxyacid synthase. *J. Biol. Chem.* **2003**, *278*, 7639–7644.
- (25) Laskowski, R. A.; MacArthur, M. W.; Moss, D. S.; Thornton, J. M. PROCHECK: A program to check the stereochemical quality of protein structures. *J. App. Cryst.* **1993**, *26*, 283–291.
- (26) Wiederstein, M.; Sippl, M. J. ProSA-web: interactive web service for the recognition of errors in three-dimensional structures of proteins. *Nucleic Acids Res.* **2007**, *35*, W407–410.
- (27) Hill, C. M.; Duggleby, R. G. Mutagenesis of *Escherichia coli* acetohydroxyacid synthase isoenzyme II and characterization of three herbicide-insensitive forms. *Biochem. J.* **1998**, *335*, 653–661.
- (28) Wang, D.; Yang, C.; Kuang, T.; Lei, H.; Meng, X.; Tong, A.; He, J. F.; Jiang, Y.; Guo, F.; Dong, M. Prevalence of multidrug and extensively drug-resistant tuberculosis in Beijing, China: A hospital-based retrospective study. *Jpn. J. Infect. Dis.* **2010**, *63*, 368–371.
- (29) LaRossa, R. A.; Schloss, J. V. The sulfonylurea herbicide sulfometuron methyl is an extremely potent and selective inhibitor of acetolactate synthase in *Salmonella typhimurium*. *J. Biol. Chem.* **1984**, *259*, 8753–8757.
- (30) McCourt, J. A.; Duggleby, R. G. Acetohydroxyacid synthase and its role in the biosynthetic pathway for branched-chain amino acids. *Amino Acids* **2006**, *31*, 173–210.
- (31) Awasthy, D.; Gaonkar, S.; Shandil, R. K.; Yadav, R.; Bharath, S.; Marcel, N.; Subbulakshmi, V.; Sharma, U. Inactivation of the *ilvB1* gene in *Mycobacterium tuberculosis* leads to branched-chain amino acid auxotrophy and attenuation of virulence in mice. *Microbiology* **2009**, *155*, 2978–2987.
- (32) Wallace, A. C.; Laskowski, R. A.; Thornton, J. M. LIGPLOT: A program to generate schematic diagrams of protein–ligand interactions. *Protein Eng.* **1995**, *8*, 127–134.
- (33) Thompson, J. D.; Higgins, D. G.; Gibson, T. J. CLUSTAL W: improving the sensitivity of progressive multiple sequence alignment through sequence weighting, position-specific gap penalties and weight matrix choice. *Nucleic Acids Res.* **1994**, *22*, 4673–4680.
- (34) *Insight II*, version 2005; Accelrys: San Diego, CA, 2005.
- (35) SYBYL, version 6.8; Tripos Associates: St. Louis, MO, 2001.
- (36) Cornell, W. D.; Cieplak, P.; Bayly, C. I.; Gould, I. R.; Merz, K. M.; Ferguson, D. M.; Spellmeyer, D. C.; Fox, T.; Caldwell, J. W.; Kollman, P. A. A second generation force field for the simulation of proteins, nucleic acids, and organic molecules. *J. Am. Chem. Soc.* **1995**, *117*, 5179–5197.
- (37) *Maestro*, version 7.5.112; Schrödinger: Portland, OR, 2000.
- (38) Huang, N.; Shoichet, B. K.; Irwin, J. J. Benchmarking sets for molecular docking. *J. Med. Chem.* **2006**, *49*, 6789–6801.
- (39) *Discovery Studio*, version 2.1; Accelrys: San Diego, CA, 2008.
- (40) Kabsch, W. A discussion of the solution for the best rotation to relate two sets of vectors. *Acta Crystallogr.* **1978**, *A34*, 827–828.

- (41) Lee, Y. T.; Duggleby, R. G. Mutagenesis studies on the sensitivity of *Escherichia coli* acetohydroxyacid synthase II to herbicides and valine. *Biochem. J.* **2000**, *350*, 69–73.
- (42) Wang, J. G.; Li, Z. M.; Ma, N.; Wang, B. L.; Jiang, L.; Pang, S. S.; Lee, Y. T.; Guddat, L. W.; Duggleby, R. G. Structure–activity relationships for a new family of sulfonylurea herbicides. *J. Comput.-Aided Mol. Des.* **2005**, *19*, 801–820.
- (43) PyMOL, version 1.3r1 edu; DeLano Scientific: Palo Alto, CA, 2010.